

Exploring Non-Abelian Geometric Phases in Spin-1 Ultracold Atoms

Bharath H. M.,^{1,2,3} Matthew Boguslawski,¹ Maryrose Barrios,¹ Lin Xin,¹ and Michael S. Chapman¹

¹*School of Physics, Georgia Institute of Technology, 837 State Street NW, Atlanta, Georgia 30332, USA*

²*Fakultät für Physik, Ludwig-Maximilians-Universität München, 4 Schellingstraße, 80799 München, Germany*

³*Max-Planck-Institut für Quantenoptik, 85748 Garching, Germany*



(Received 9 April 2019; published 24 October 2019)

The spin vector of a spin-1 system, unlike that of a spin-1/2 system, can lie anywhere on or inside the Bloch sphere representing the phase space. As a consequence, the geometrical and topological properties of the spin-1 phase space of quantum states are richer and require a generalization of Berry's phase. For special trajectories passing through the center of the Bloch sphere (*singular loops*), the geometric phase has a non-Abelian nature. Here, we experimentally explore this geometric phase for singular loops in a spin-1 quantum system using ultracold ⁸⁷Rb atoms confined in an optical trap using microwave and rf control fields.

DOI: [10.1103/PhysRevLett.123.173202](https://doi.org/10.1103/PhysRevLett.123.173202)

Berry's geometric phase is a manifestation of the geometrical and topological properties of the state space (or parameter space) of a physical system, with no regard to its dynamics. Although, the condition of *adiabaticity* [1] speaks of the dynamics, it was later established that this condition is dispensable [2,3], and it is a kinematic property [4]. For instance, fully magnetized spin states live on a sphere, known as the Bloch sphere and the corresponding Berry's phase is a manifestation of the geometry and topology of a sphere. In contrast, zero magnetization states of an integer spin system do not live on a sphere—they live on the *real projective plane* ($\mathbb{R}P^2$), the space of all diameters of a sphere. As a consequence, the Berry phase of the zero magnetization states is a manifestation of the topology of $\mathbb{R}P^2$ [5]. Recent theoretical work [6] has revealed interesting features of the space of spin-1 quantum states, developing a non-Abelian geometric phase for loops inside the Bloch sphere, that also derives its properties from the topology of $\mathbb{R}P^2$.

Owing to its geometrical origin, Berry's phase for spin-1/2 systems is robust to dynamical fluctuations and can be used to construct robust phase gates known as *holonomic gates* [7–11]. Adiabatic as well as nonadiabatic, non-Abelian holonomic gates in two-level systems have been demonstrated using nitrogen-vacancy centers [12–15], and transmons [16,17]. More recently, optically controlled holonomic gates have been implemented in nitrogen-vacancy centers [18,19], ion traps [20,21], and nuclear magnetic resonance systems [22]. Although many of the above experiments used an ancillary level in addition to the qubit states and therefore involved qutrit manipulations effectively, the geometric phase loops themselves were always confined to a qubit subspace. Therefore, the geometric and topological properties exclusive to the space of spin-1 quantum states remains experimentally unexplored.

Here, we report on the first experimental observation, using ultracold ⁸⁷Rb atoms, of the non-Abelian SO(3) geometric phase, unique to spin-1 and higher systems [6]. Besides deriving its properties from the topology of $\mathbb{R}P^2$, this geometric phase is richer than Berry's phase in many other ways: It is defined for all loops on or inside the Bloch sphere, spanning the full qutrit space and it is carried not by the overall phase, but by the tensor of spin fluctuations. The latter, represented by a 3D ellipsoid, provides a useful geometric perspective on the properties of spin-1 quantum states.

The quantum state of a spin-1/2 system is uniquely represented by a point on the Bloch sphere whose coordinates are given by the expectation values of the spin operators S_x , S_y , and S_z . Spin-1 (and higher) quantum states differ in two ways. First, the expectation value of the spin vector $\vec{S} = (\langle S_x \rangle, \langle S_y \rangle, \langle S_z \rangle)^T$ is not confined to the surface of the Bloch sphere; it could be anywhere on or *inside* the Bloch sphere. And second, a quantum state is not uniquely represented by its spin vector; there can be multiple quantum states that share the same spin vector. For spin-1 systems, this ambiguity is resolved by considering the quantum fluctuations of the spin vector, i.e., an ellipsoid surrounding the head of the spin vector [Fig. 1(a)]. This ellipsoid represents a rank two tensor (T), also known as the covariance matrix, whose components are $T_{ij} = \frac{1}{2}(\langle S_i S_j \rangle - \langle S_i \rangle \langle S_j \rangle)$. The pair (\vec{S}, T) uniquely represents a spin-1 quantum state up to an overall phase [23].

The geometric phase arises in this system when the ellipsoid is parallel transported along a closed loop inside the Bloch sphere [Figs. 1(c) and 1(d)]. As a result of the parallel transport, the ellipsoid returns in a different orientation which can be described by a 3D rotation, represented by a 3×3 matrix. This rotation matrix (R), a member of the non-Abelian SO(3) group, is the

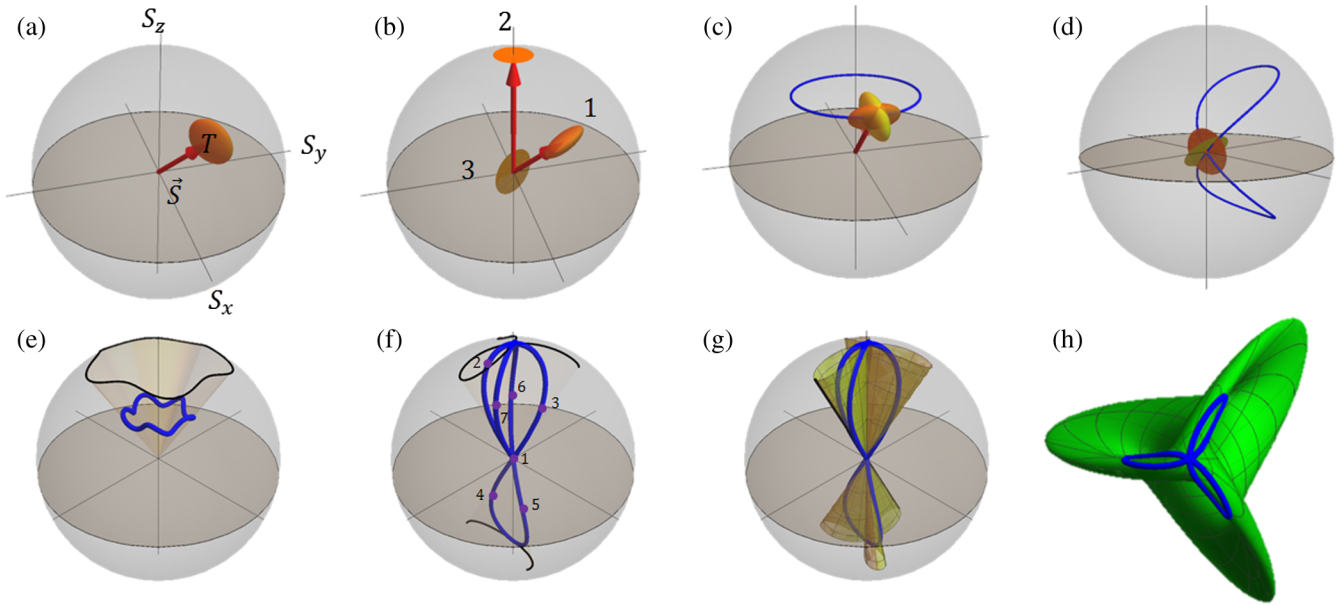


FIG. 1. Theory of spin-1 geometric phases: (a) shows that the spin vector (\vec{S}) and the spin fluctuation tensor (T) can together be represented by a point inside the Bloch sphere surrounded by an ellipsoid. (b) illustrates that the lengths of the ellipsoid's axes are constrained by the length of the spin vector. Explicitly, they are given by $\sqrt{1 - |\vec{S}|^2}$ and $\sqrt{(1 \pm \sqrt{1 - |\vec{S}|^2})/2}$. For the three examples labeled 1, 2, and 3, the spin vectors $\vec{S}_{1,2,3}$ satisfy $0 < |\vec{S}_1| < 1$, $|\vec{S}_2| = 1$, and $|\vec{S}_3| = 0$. The ellipsoid degenerates to a disk for the last two cases. (c) and (d) show the geometric phases carried by the ellipsoid when it is parallel transported along a nonsingular and a singular loop inside the Bloch sphere, respectively. The final orientation of the ellipsoid is different from the initial orientation, due to an $SO(3)$ geometric phase. (e) and (f) contrast nonsingular and singular loops under a radial projection. The former has a continuous projection and a well-defined solid angle, while the latter does not. (g) shows a diametric projection of the loop. The solid angle enclosed by this cone is the generalized solid angle of the singular loop. This surface is indeed a loop in the space of diameters of a sphere, i.e., in $\mathbb{R}P^2$. (h) shows a Boy's surface, a representation of $\mathbb{R}P^2$, together with the loop projected on it. The generalized solid angle is equal to the holonomy of this loop.

geometric phase of the loop. This geometric phase is an operator, unlike Berry's phase which is a complex scalar, and is therefore more similar to the Wilczek-Zee phase [27] and the Uhlmann phase [28]. This can be measured easily in the components of the spin fluctuation tensor, specifically, the component T_{ij} changes to $R_{il}T_{lk}R_{jk}$ after the parallel transport, a non-Abelian transformation.

The parallel transport of the ellipsoid has a deep geometrical significance to the abstract space of quantum states. The Fubini-Study metric, also known as the "quantum angle," characterizes the geometry of the space of quantum states [29]. Among the infinitely many ways of transporting the ellipsoid along a loop inside the Bloch sphere, the parallel transport is the one that minimizes the Fubini-Study length of the resulting path in the space of quantum states [30–32]. Loops (not) passing through the center are called (non)singular loops.

Geometrical interpretation of this geometric phase, particularly for singular loops, needs the notion of *generalized solid angles* [6]. The parallel transport of the ellipsoid inside the Bloch sphere along a nonsingular loop is reminiscent of the parallel transport of a tangent vector to a sphere. Its geometric phase is therefore a rotation about

the spin vector by an angle equal to its solid angle [Fig. 1(e)] and is Abelian. This solid angle is the angle of the cone obtained by sweeping a radius along the loop [Fig. 1(e)]. This cone is the *radial projection* of the loop. For singular loops, this geometric notion of solid angle is not well defined, as illustrated in Fig. 1(f). The radial projection is discontinuous.

The discontinuous jumps in the radial projection of singular loops are always diametrically opposite and therefore, sweeping a diameter along the loop generates a continuous cone (i.e., a *diametric projection*), with a well-defined angle [Fig. 1(g)]. This angle is equal to the standard solid angle for nonsingular loops and is a convenient generalization to singular loops.

While the standard solid angle is the integrated curvature or *holonomy* of a loop on a sphere, the generalized solid angle is the holonomy of a loop on $\mathbb{R}P^2$ [23]. The diametric projection of a loop inside the Bloch sphere is a path in $\mathbb{R}P^2$. The holonomy of this path is indeed equal to the generalized solid angle [6]. $\mathbb{R}P^2$ can be represented by a self-intersecting surface, known as Boy's surface [33] [Fig. 1(h)]. If the projection on $\mathbb{R}P^2$ is open, its holonomy is defined after closing it with a geodesic [Fig. 2(c)] [23].

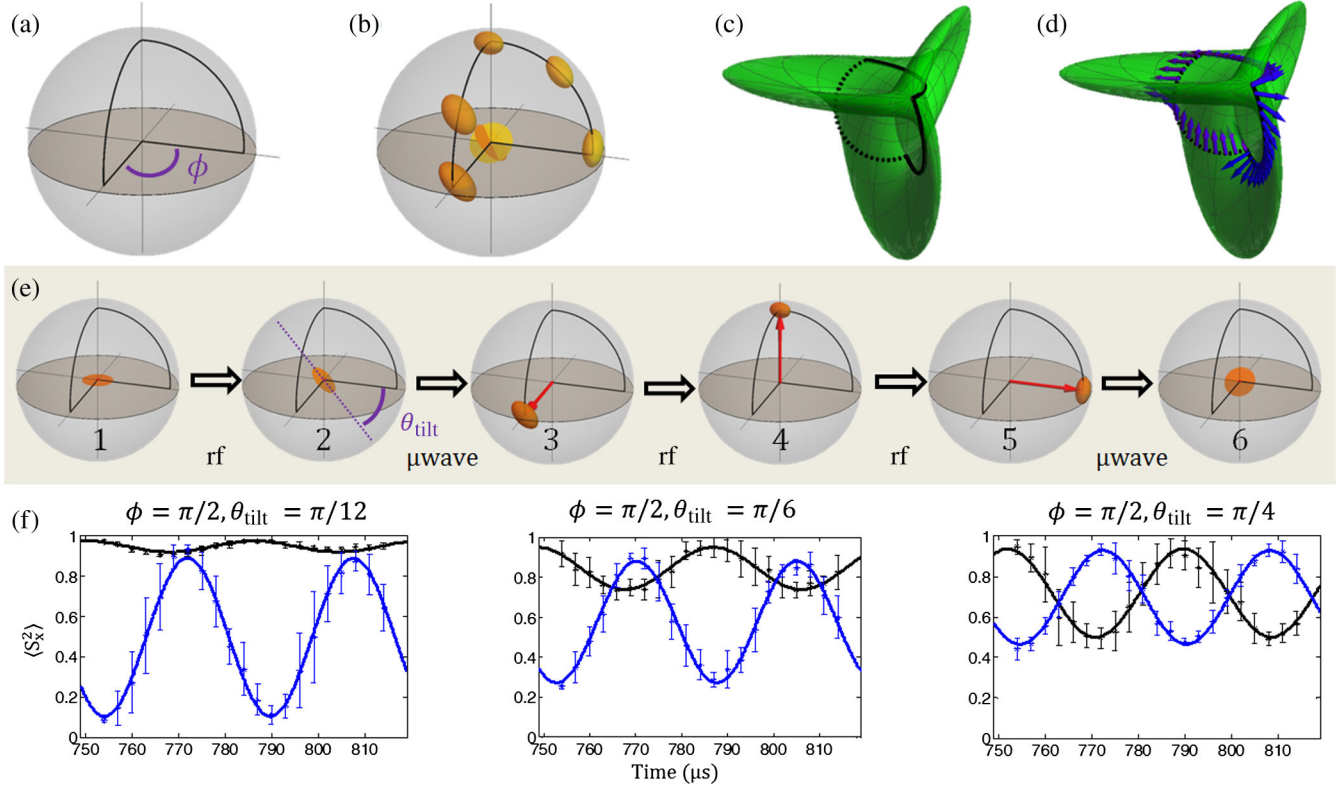


FIG. 2. Experimental sequence. (a) shows a singular loop that we implement experimentally. (b) shows how an ellipsoid is parallel transported along this loop. (c) shows its projection on $\mathbb{R}P^2$. This projection is an open path and its holonomy is defined after closing it with a geodesic [34,35], shown by the dashed curve. (d) illustrates the holonomy of this path, i.e., the angle of rotation of a unit tangent vector, after it is parallel transported along this loop. The experimental sequence of transporting the ellipsoid along this loop inside the Bloch sphere is illustrated in (e). In order to observe the geometric phase, we measure S_x^2 as the tilted disk spins about the z axis at the Larmor rate. (f) shows the oscillation of S_x^2 without (black) and with (blue) the transport along the loop. The geometric phase is encoded in the phase shift and the amplitude shift between the black and the blue datasets. Each data point is an average of ten shots and the error bars represent the standard deviation.

The diametric projection also equips us with a concise way of determining the geometric phase operator R . The two end points of the diameter trace out a pair of congruent loops on the surface of the Bloch sphere, which we may parametrize in time as $+\hat{n}(t)$ and $-\hat{n}(t)$, respectively. The geometric phase then is

$$R = \mathcal{T} \exp \left(\int (\hat{n}\hat{n}^T - \hat{n}\hat{n}^T) dt \right). \quad (1)$$

Here, \mathcal{T} is the time ordering operator and the integral is evaluated through the loop.

We now turn to the experimental measurements. The experiments are performed in the $F = 1$ hyperfine level of the electronic ground state of ultracold ^{87}Rb atoms in an optical dipole trap. A cloud of about 20 000 atoms evaporatively cooled to $<1 \mu\text{K}$ are initialized in the $m_F = 0$ state [23,36]. From this starting point, any path within the Bloch sphere can be induced by a combination of rotating (rf) magnetic field pulses and microwave 2π pulses connecting the $F, M_F = 1, 0 \rightarrow 2, 0$ states. The former generates the

familiar Rabi rotation of the spin [23], and the latter realizes a quadrupole operator that changes the spin length [37,38]. The final state of the system is determined by measuring the populations in $m_F = 0, \pm 1$ using a Stern-Gerlach separation of the cloud followed by fluorescence imaging of the atoms [37]. This provides a direct measurement of $\langle S_z \rangle$ and $\langle S_z^2 \rangle$. The transverse components of the spin length and moments, e.g., $\langle S_x^2 \rangle$, are measured using a $\pi/2$ rf pulse preceding the Stern-Gerlach separation.

We use the class of singular loops that start and end at the center shown in [Fig. 2(a)]. They capture the distinguishing features of this geometric phase, and are also convenient to realize experimentally. The experimental sequence [Fig. 2(e)] begins with an rf pulse that tilts the flat disk, i.e., the initial state by the desired angle θ_{tilt} . We then induce a transport along the loop using a sequence of microwave and rf pulses. In a frame rotating at the Larmor frequency, a resonant rf field is a constant field while the microwave fields are insensitive to the Larmor rotation. Therefore, the pulse sequence shown in Fig. 2(e) effectively induces the loop in the rotating frame.

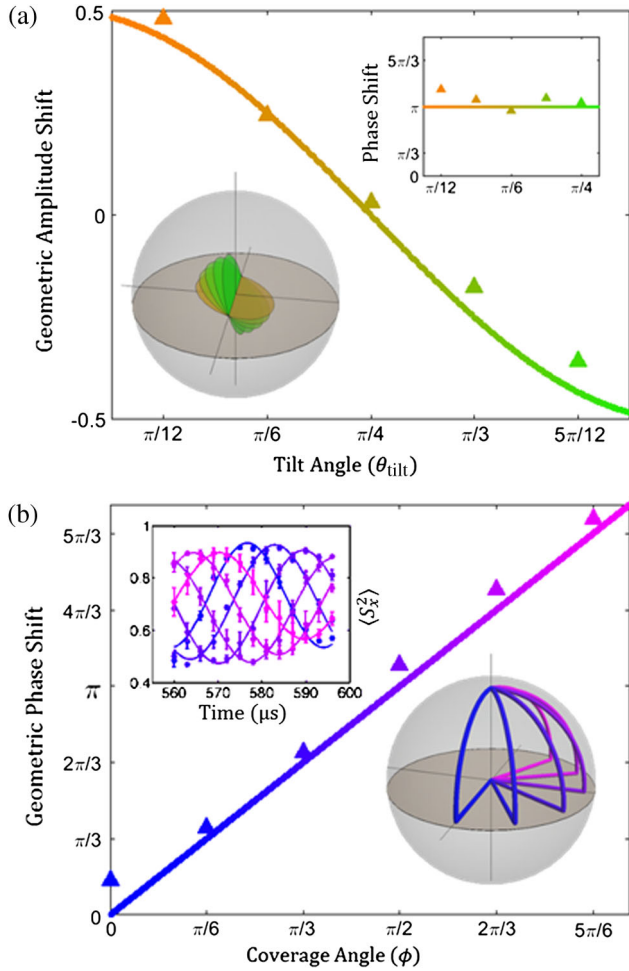


FIG. 3. Geometric amplitude shift and phase shift: (a) shows the theoretical (continuous curve) and the experimental (triangular markers) geometric amplitude shifts. The top inset shows the geometric phase shifts for these five tilt angles and the continuous line shows the corresponding theoretical value, i.e., π . The bottom inset shows the disks (magnified) at the starting point with different tilt angles used in the experiment. (b) shows the theoretical (continuous curve) and experimental values (triangular markers) of the geometric phase shift for different values of the coverage angle (ϕ). The upper inset shows the corresponding Larmor oscillation of $\langle S_x^2 \rangle$. The lower inset shows the loops corresponding to the different values of ϕ used in the experiment. The error bars corresponding to the above data points (i.e., fit parameters) range between 0.012 and 0.03, smaller than the markers and therefore are not displayed.

The geometric phase and the generalized solid angle are $R = R_z(\phi)R_x(-\phi)$ and ϕ , respectively, for these loops [23]. The initial state is a disk tilted about the x axis by an angle θ_{tilt} . When this disk is parallel transported along this loop, the geometric phase R manifests as a different final orientation of the disk, now tilted about $\hat{x}' = \hat{x} \cos \phi + \hat{y} \sin \phi$, by an angle $\theta'_{\text{tilt}} = \phi + \theta_{\text{tilt}}$.

Because of the Larmor precession, $\langle S_x^2 \rangle$ oscillates at twice the Larmor frequency (ω_L). If a disk is tilted by

θ_{tilt} about the x axis at $t = 0$, then $\langle S_x^2(t) \rangle = 1 - \sin^2 \theta_{\text{tilt}} \sin^2(\omega_L t)$. After the parallel transport, $\langle S_x^2(t) \rangle = 1 - \sin^2 \theta'_{\text{tilt}} \sin^2(\omega_L t + \phi)$. That is, due to its non-Abelian nature, the accumulated geometric phase can be observed in two parameters—a phase shift of 2ϕ as well as an amplitude shift of $\sin^2 \theta_{\text{tilt}} - \sin^2 \theta'_{\text{tilt}}$ in the oscillation of $\langle S_x^2(t) \rangle$.

The transport induced by the rf pulse is naturally a parallel transport; i.e., the rf field evolves the system along the path of least Fubini-Study length [7]. However, this is not true for the microwave pulses; the transport along the straight segments is not parallel and the system is taken along a path of nonminimal Fubini-Study length [23]. Consequently, some dynamical phase is accumulated during this transport that needs to be measured in order to isolate the geometric phase. To accomplish this, we take two data sets each measuring the oscillation of $\langle S_x^2 \rangle$ —one after transporting the disk along the loop and another after transporting the disk radially outward and then back inward, for which there is no geometric contribution. A comparison of these two data sets allows determination of the geometric phase shift and amplitude shift of the induced loops [Fig. 2(f)].

We have measured both the geometric phase shifts and amplitude shifts for a range of angles ($\theta_{\text{tilt}}, \phi$), as shown in Fig. 3. In Fig. 3(a), we investigate loops with a fixed angle $\phi = (\pi/2)$ for different initial orientations of the disk θ_{tilt} in order to demonstrate a nontrivial amplitude shift. The theoretical phase shift in the oscillation of $\langle S_x^2 \rangle$ is $2\phi = \pi$ for each of the initial orientations of the disk, and the experimental values are in good agreement, as seen in the inset of Fig. 3(a). The theoretical amplitude shift depends on the initial disk orientation—it is $(1/2) \cos 2\theta_{\text{tilt}}$. The observed amplitude shift is in excellent agreement with the theory [Fig. 3(a)]. Data sets with explicit sinusoidal fits showing the phase shift and amplitude shift corresponding to three of the different initial orientations are shown in Fig. 2(f).

In Fig. 3(b), we demonstrate the dependence of the phase shift to the generalized solid angle of the loop. For these measurements, the starting disk orientation is $\theta_{\text{tilt}} = (\pi/4)$ and the range of loops investigated is shown in the inset to the figure. The measured phase shifts show excellent agreement with the theoretical phase shift in the oscillation of $\langle S_x^2 \rangle$, which is 2ϕ .

Unlike Abelian geometric phases, this geometric phase manifests in terms of two observable parameters—the phase shift and the amplitude shift. Using a set of loops, all of them based at the center, we have shown the variation of the amplitude shift at constant phase shift in one dataset [Fig. 3(a)] and the variation of the phase shift at constant amplitude shift in the other [Fig. 3(b)]. That is, these two parameters vary independently implying that the group of geometric phase operators is more complicated than the Abelian group of all rotations about a fixed axis. There are

no two parameter Abelian subgroups in the group of all rotations, i.e., $SO(3)$. Therefore, our experimental data demonstrate the non-Abelian nature of this geometric phase, which occurs only for singular loops [6].

We have experimentally demonstrated the non-Abelian geometric phases carried by the spin fluctuation tensor in spin-1 systems. We have also measured directly, the generalized solid angle of the singular loops considered here. This is the first experiment exploring the nontrivial topological properties of spin-1 quantum systems, that arise from $\mathbb{R}P^2$. A natural succession of our experiment is to prepare 1D and 2D spin textures in spatially extended spin-1 systems. Spin-1/2 textures like skyrmions, domain walls, and Néel walls have been extensively studied and are characterized by their Berry phase. Spin-1 quantum states add a new feature to these textures—the spin vector can be inside the Bloch sphere, allowing for a larger class of textures.

We hope that this geometric phase will find applications in studying topological phase transitions [39] in systems with a complex tensor order [40], which transforms similar to the spin fluctuation tensor under $SO(3)$ rotations.

We thank John Etnyre, T. A. B. Kennedy, Carlos Sá de Melo, and Shubhayu Chatterjee for fruitful discussions and insights. We also acknowledge support from the National Science Foundation, Grant No. NSF PHYS-1806315.

-
- [1] M. V. Berry, *Proc. R. Soc. A* **392**, 45 (1984).
 [2] Y. Aharonov and J. Anandan, *Phys. Rev. Lett.* **58**, 1593 (1987).
 [3] B. Simon, *Phys. Rev. Lett.* **51**, 2167 (1983).
 [4] N. Mukunda and R. Simon, *Ann. Phys. (N.Y.)* **228**, 205 (1993).
 [5] J. M. Robbins and M. V. Berry, *J. Phys. A* **27**, L435 (1994).
 [6] H. M. Bharath, *J. Math. Phys. (N.Y.)* **59**, 062105 (2018).
 [7] E. Sjöqvist, V. Azimi Mousolou, and C. M. Canali, *Quantum Inf. Process.* **15**, 3995 (2016).
 [8] A. Y. Kitaev, *Ann. Phys. (Amsterdam)* **303**, 2 (2003).
 [9] P. Zanardi and M. Rasetti, *Phys. Lett. A* **264**, 94 (1999).
 [10] E. Sjöqvist, *Phys. Lett. A* **380**, 65 (2016).
 [11] G. F. Xu, C. L. Liu, P. Z. Zhao, and D. M. Tong, *Phys. Rev. A* **92**, 052302 (2015).
 [12] C. G. Yale, F. J. Heremans, B. B. Zhou, A. Auer, G. Burkard, and D. D. Awschalom, *Nat. Photonics* **10**, 184 (2016).
 [13] C. Zu, W.-B. Wang, L. He, W.-G. Zhang, C.-Y. Dai, F. Wang, and L.-M. Duan, *Nature (London)* **514**, 72 (2014).
 [14] S. Arroyo-Camejo, A. Lazariev, S. W. Hell, and G. Balasubramanian, *Nat. Commun.* **5**, 4870 (2014).
 [15] K. Nagata, K. Kuramitani, Y. Sekiguchi, and H. Kosaka, *Nat. Commun.* **9**, 3227 (2018).
 [16] P. J. Leek, J. M. Fink, A. Blais, R. Bianchetti, M. Göppl, J. M. Gambetta, D. I. Schuster, L. Frunzio, R. J. Schoelkopf, and A. Wallraff, *Science* **318**, 1889 (2007).
 [17] A. A. Abdumalikov, Jr., J. M. Fink, K. Juliusson, M. Pechal, S. Berger, A. Wallraff, and S. Filipp, *Nature (London)* **496**, 482 (2013).
 [18] Y. Sekiguchi, N. Niikura, R. Kuroiwa, H. Kano, and H. Kosaka, *Nat. Photonics* **11**, 309 (2017).
 [19] B. B. Zhou, P. C. Jerger, V. O. Shkolnikov, F. J. Heremans, G. Burkard, and D. D. Awschalom, *Phys. Rev. Lett.* **119**, 140503 (2017).
 [20] K. Toyoda, K. Uchida, A. Noguchi, S. Haze, and S. Urabe, *Phys. Rev. A* **87**, 052307 (2013).
 [21] D. Leibfried, B. DeMarco, V. Meyer, D. Lucas, M. Barrett, J. Britton, W. M. Itano, B. Jelenković, C. Langer, T. Rosenband, and D. J. Wineland, *Nature (London)* **422**, 412 (2003).
 [22] G. Feng, G. Xu, and G. Long, *Phys. Rev. Lett.* **110**, 190501 (2013).
 [23] See Supplemental Material at <http://link.aps.org/supplemental/10.1103/PhysRevLett.123.173202> for details, which includes Refs. [24–26].
 [24] F. Bloch and A. Siegert, *Phys. Rev.* **57**, 522 (1940).
 [25] J. Spiegelberg and E. Sjöqvist, *Phys. Rev. A* **88**, 054301 (2013).
 [26] H. M. Bharath, Ph. D. thesis, School of Physics, Georgia Institute of Technology, 2018.
 [27] F. Wilczek and A. Zee, *Phys. Rev. Lett.* **52**, 2111 (1984).
 [28] A. Uhlmann, *Rep. Math. Phys.* **24**, 229 (1986).
 [29] I. Bengtsson and K. Życzkowski, *Geometry of Quantum States: An Introduction to Quantum Entanglement* (Cambridge University Press, Cambridge, England, 2006).
 [30] A. Uhlmann, *Rep. Math. Phys.* **36**, 461 (1995).
 [31] P. M. Alberti and A. Uhlmann, *Acta Appl. Math.* **60**, 1 (2000).
 [32] A. K. Pati, *Phys. Lett.* **159A**, 105 (1991).
 [33] F. Apery, *Models of the Real Projective Planes* (Vieweg+Teubner Verlag, Wiesbaden, 1987).
 [34] J. Samuel and R. Bhandari, *Phys. Rev. Lett.* **60**, 2339 (1988).
 [35] S. Pancharatnam, *Proc. Indian Acad. Sci. A* **44**, 247 (1956).
 [36] W. Zhang, D. L. Zhou, M.-S. Chang, M. S. Chapman, and L. You, *Phys. Rev. Lett.* **95**, 180403 (2005).
 [37] T. M. Hoang, H. M. Bharath, M. J. Boguslawski, M. Anquez, B. A. Robbins, and M. S. Chapman, *Proc. Natl. Acad. Sci. U.S.A.* **113**, 9475 (2016).
 [38] C. D. Hamley, C. S. Gerving, T. M. Hoang, E. M. Bookjans, and M. S. Chapman, *Nat. Phys.* **8**, 305 (2012).
 [39] E. Witten, *Nuovo Cimento Riv. Ser.* **39**, 313 (2016).
 [40] I. Boettcher and I. F. Herbut, *Phys. Rev. B* **97**, 064504 (2018).